Chapter 13
The SOLENE-Microclimat Model: Potentiality for Comfort and Energy Studies

Marjorie Musy, Marie-Hélène Azam, Sihem Guernouti, Benjamin Morille, and Auline Rodler

13.1 Introduction

Conducting full-scale experiments in the actual urban context is a difficult task. This is why simulation is needed to test planning and urban design proposals and to predict the impacts of urban developments on local climate and building thermal behavior.

It is necessary therefore to build models that are robust enough and capable of simulating realistic urban settings, including buildings. When examining urban comfort, the scale considered is that of the immediate environment, i.e., street and square. Urban form is the most important parameter that acts on the local climate. It is the reason why its explicit description (including buildings, trees, etc.) is a necessary input into microclimate models. The primary outputs of the models are in return their impacts on sunlight, wind, air temperature, and humidity as well as surface temperature.

SOLENE-microclimat was developed to assess the impact of urban planning on both outdoor and indoor comfort taking into account the interactions between a building and its environment. This requires resolving scale compatibility issues

M. Musy (✉) · S. Guernouti · A. Rodler
Buildings Performance in their Environment (BPE) Research Team, Cerema Ouest & Institut de Recherche en Sciences et Techniques de la Ville (IRSTV), FR CNRS 2488, Nantes, France
e-mail: marjorie.musy@cerema.fr; sihem.guernouti@cerema.fr; auline.rodler@cerema.fr

M.-H. Azam
UMR CNRS 6£183, GeM, Univeristé de Nantes & Institut de Recherche en Sciences et Techniques de la Ville (IRSTV), FR CNRS 2488, Nantes, France
e-mail: marie-helene.azam@univ-nantes.fr

B. Morille
Soleneos & Institut de Recherche en Sciences et Techniques de la Ville FR CNRS 2488, Nantes, France
e-mail: benjamin.morille@soleneos.fr

M. Palme, A. Salvati (eds.), *Urban Microclimate Modelling for Comfort and Energy Studies*, https://doi.org/10.1007/978-3-030-65421-4_13

given the difficulty to accurately represent the urban environment as well as the buildings and their uses within the same tool.

Only a full coupling between building energy models and urban microclimate models allows to:

- Evaluate the reciprocal impact between the urban environment and the thermal behavior of buildings
- Obtain direct and indirect impacts of the selected adaptation techniques
- Better estimate the heat released in the city due to the indoor space thermal control

13.2 The SOLENE-Microclimat Model: Principle

SOLENE-microclimat was first developed for outdoor comfort assessment (Vinet et al. 1999). The addition of new sub-models makes it possible to take into account (1) radiative transfers, including long-wave radiation; (2) conduction and storage in walls and soils; (3) airflow and convective exchanges; (4) evapotranspiration from natural surfaces like vegetation and water ponds or watering systems; and (5) energy balance (energy demand or indoor temperature) for a building in the simulated area. Point 1 corresponds to the historical SOLENE radiative model and can be run alone. Points 1+2 correspond to the thermo-radiative model based on SOLENE (addition of the thermal modeling of different kinds of surfaces). It can also be run independently. Points 1+2+3+4+5 correspond to the so-called SOLENE-microclimat model (Fig. 13.1). For the moment, only the anthropogenic flux due to the heating or cooling of buildings is taken into account.

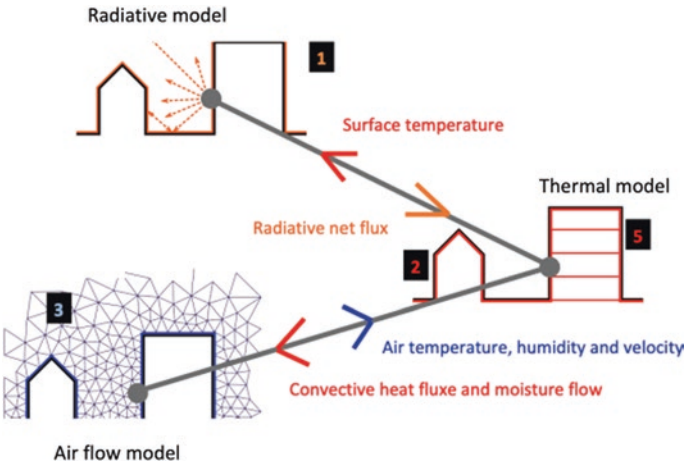

Fig. 13.1 The coupling of the three different models (radiative model = SOLENE, thermal model for urban surfaces and buildings, airflow model = Code_Saturne). Results that are passed from a model to another are represented by colored arrows. Point 4 is not represented; evapotranspiration is taken into account in the energy balance equation used to link all fluxes

This complete coupling of models has not yet been validated, although some comparisons have been attempted by Athamena (2012) on a street canyon composed of containers, showing good agreement for both air temperature and velocity in the street.

In this chapter, we present the modules that compose SOLENE-microclimat and how they can be used to study the direct and indirect impacts of adaptation and mitigation solutions. SOLENE-microclimat consists of the following modules:

- A thermo-radiative module that calculates the thermal behavior and the radiative exchange of urban impervious surfaces (roofs, wall, and pavement), considering their albedo and emissivity properties. This model allows for assessing the impact of cool materials.
- Modules that compute the evaporation and heat fluxes for water ponds, vegetation (trees, lawns, green roofs, green walls), and pavement watering.
- Modules that are used to assess the impacts (thermal comfort assessment and building energy simulation).

For each sub-module, the model it is based on is first described. Then, its validation process when performed is presented. The confidence and credibility of a physical model lie on its validation. However, validation is a complex task when trying to do it for the whole model. It is why a systemic approach was adopted. Most modules implemented in SOLENE-microclimat have been assessed separately instead of assessing the whole model on a variable that integrates all the phenomena such as the atmosphere temperature, as often done. We have considered that this last method would not allow us to conclude on the model's ability to accurately represent each phenomenon. Surface temperatures and temperatures in materials can be accurately measured and their variability in an urban scene allows to assess the model for different conditions (radiative characteristics, materials …) and then to conclude on the submodels' accuracy. This chapter describes the equations and assumptions that are made, their verification, and the validation steps. This valuable information is intended to support the work of researchers and practitioners interested in this model to fully understand its architecture and functioning as well as developers of other tools.

13.3 The Thermo-Radiative Model

13.3.1 Model Description

The *SOLENE-microclimat* simulation tool calculates the solar and luminous effects, due to urban forms and materials and long-wave radiation, conduction, and storage in built surfaces. The model is based on a 3D representation of urban geometry (Fig. 13.2).

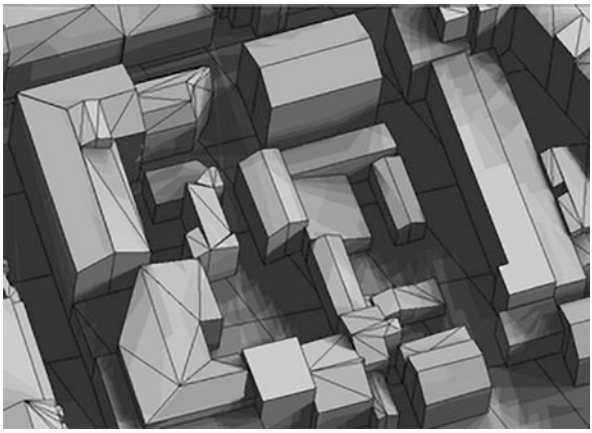

Fig. 13.2 3D model of small district in SOLENE (with sun projections over a 1-day period)

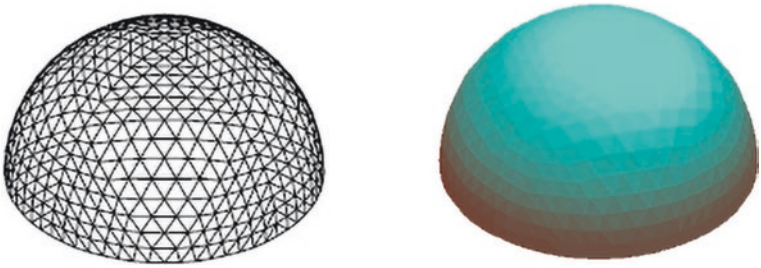

Fig. 13.3 Sky vault representation

The simulated scenes are modeled by the meshing of the 3D developed surface with rectangular or triangular elements, whose area depends on the size of the simulated scene. An additional hemispherical geometry represents the sky vault, which is meshed to take into account the anisotropy of the diffuse solar radiation (Fig. 13.3). The radiation spectrum is divided into two bands corresponding to solar radiation (short wave, SW) and infrared thermal radiation (long wave, LW). The direct solar radiation is emitted by the sky mesh in the sun direction, while the diffuse solar radiation emission is distributed over all sky vault facets by a sky radiance model (Perez et al. 1987). The sky thermal radiation is assumed to be isotropic. These data can be replaced by measurement data if available.

At each time step, the SW radiation absorbed by each facet (R_{n_SW}) is computed as the result of the direct and diffuse SW radiation received directly from the sun and sky (resp. R_{direct_SW} and $R_{diffuse\_SW}$), plus reflections from all other facets in view (R_{IR_SW}), weighted by the absorption coefficient of the surface (Eq. 13.1):

$$R_{n-SW} = \alpha_i \left(R_{direct-SW} + R_{diffuse-SW} + R_{IR-SW} \right) \tag{13.1}$$

These multiple reflections are computed according to a radiosity method that requires (1) computing geometric form factors between all facets of the built surface and the sky vault using contour integral technique (Miguet and Groleau 2002; Vinet 2000), and (2) assigning radiative properties (reflection, transmission, and absorption) to all surfaces of the scene.

The form factors are also used to calculate the net LW radiative with the surrounding surface (noted $R_{\text{n-LW}}$) (Eq. 13.2) and with the sky (noted $R_{\text{n-LW,sky}}$):

$$R_{\text{n-LW}} = \sum_{p}^{j=1} \sigma F_{ij} \left(\varepsilon_j Ts_j^4 - \varepsilon_i Ts_i^4 \right) \tag{13.2}$$

Then the net radiative flux is the sum of SW and LW net fluxes (Eq. 13.3):

$$R_{\text{n}} = R_{\text{n-SW}} + R_{\text{n LW}} + R_{\text{n-LW,sky}} \tag{13.3}$$

These fluxes are integrated into the energy budget that is calculated for all facets, writing the balance of net radiative flux, convective heat flux, and heat flux by conduction through materials behind the facet (Eq. 13.4):

$$Q_{\text{cond}} = R_{\text{n}} + H - \text{LE} \tag{13.4}$$

The convective heat flux to this atmosphere is computed using surface-to-air temperature difference and a convective heat transfer coefficient (CHTC), which can be a constant value or dependent on wind velocity at a reference point using the law proposed by Jayamaha et al. (1996) (Eq. 13.5). The 1D conductive heat flux through the walls is computed by means of a multilayer model including heat storage in the layers, conduction through the layers (as a function of the material thermal properties), and convection between the wall and an air node inside the building. This temperature is assigned in relation to indoor control temperature (Fig. 13.4). Heat transfer through ground layers and into the deep ground is computed similarly:

$$h_{\text{a}\infty} = 5.85 + 1.7 \cdot V_{\text{a}} \tag{13.5}$$

For applications focusing on soil surface temperature, for example, to assess the impact of local solutions such as watering, it appeared that the rough soil model that is usually used in SOLENE-microclimat lacked accuracy. An alternative detailed soil model has then been designed. Both of these soil models calculate the heat transfer through the layers but neglect the moisture transfer. The difference is that the detailed model is solved by a finite difference method with a nonuniform mesh, finer at the surface than deep in the ground (Fig. 13.5). At the surface, the upper boundary condition is defined by the surface energy balance. In this model, the convective heat flux method has been modified, to take into account mixed convection. Indeed, we have established that it was necessary when wanting to achieve a sufficient accuracy for surface temperature calculation whatever the wind regime. A detailed description of this soil model can be found in Azam et al. (2018b).

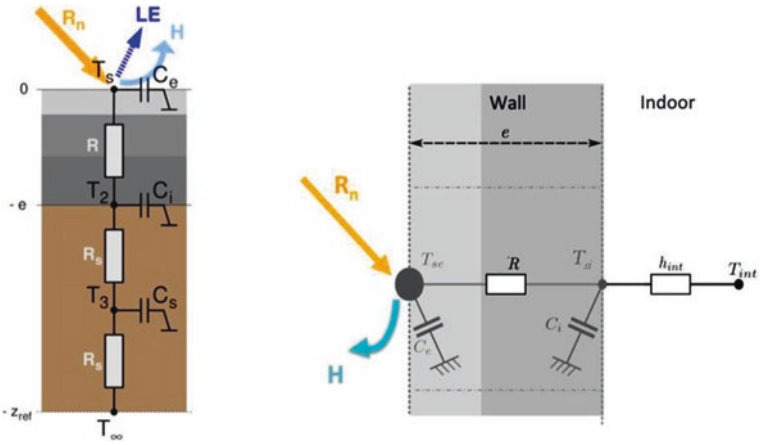

Fig. 13.4 Wall model (right) and ground models (left)

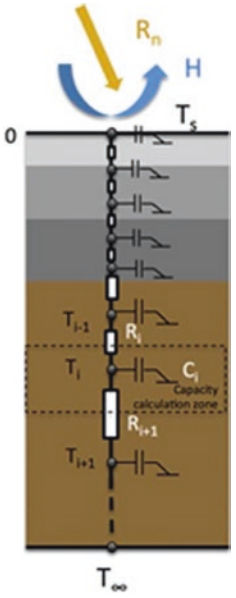

Fig. 13.5 Detailed soil model. Each color from gray to brown represents the soil layers' material variation. The capacity is estimated for each half volume above and under a capacity node

The external surface temperature of each facet (soils, buildings, etc.) is tied to that of all the other facets via long-wave radiation calculation. It results in a nonlinear system of equations that is solved by a Newton-Raphson iterative scheme at each time step.

13.3.2 Model Assessment

Hénon et al. compared simulation results carried out with this thermo-radiative model to temperatures obtained from an airborne thermal camera at facet and pixel scales (Hénon et al. 2012a, b). Measurements were acquired during two intense observation periods in summer and winter over the center of Toulouse (France). The spatial resolution (pixel size at ground) of the thermal images ranging between 1.5 and 3.0 m for zenith viewing angles between 48° and 62° allowed a manual point-to-point comparison with the temperatures calculated for the triangular mesh elements of the model, the dimension of which was about 2 m^2.

Two-thirds of pixels were simulated to within 5 °C and the other third to within 2.5 °C from actual measurements. Differences were mainly attributed to the fact that some surface types were not present in the model. Indeed, the detailed data of all surfaces in the scene were not readily available, in particular inner layers of walls and indoor temperature. Moreover, numerous smaller details cannot be represented.

This second validation step used selected measurement data acquired during the FluxSap campaign (Mestayer et al. 2011). The campaign was carried out over 3 months at a large district scale and we focused on the data acquired on a five-story building built at the beginning of the 1960s and on surrounding lawns (Fig. 13.6). The kind of measurement will be given for each surface in the following. After a survey of the surface materials, Malys (2012) compared the measured and simulated temperatures for a group of points (on a roof, on a wall, and in the ground) over several days.

For simulations, we used the weather data acquired on the roof of the building (air temperature, velocity, and humidity, SW and LW radiations). For SW radiation, as we only have the global value (diffuse and direct), when the total flux is higher than 50% of the theoretical total flux calculated for a clear sky, the flux is distributed between diffuse and direct according to Perez model for a clear sky. When it is under 50%, the flux is split into two equal parts.

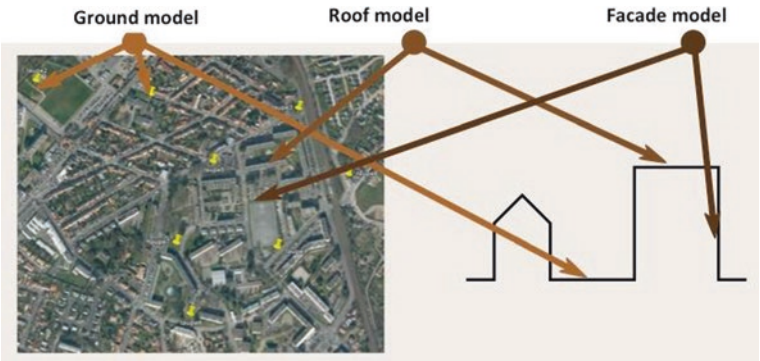

Fig. 13.6 Measurement points and their use for validating the SOLENE-microclimat model surfaces and soil temperature prediction. (Adapted from Malys 2012)

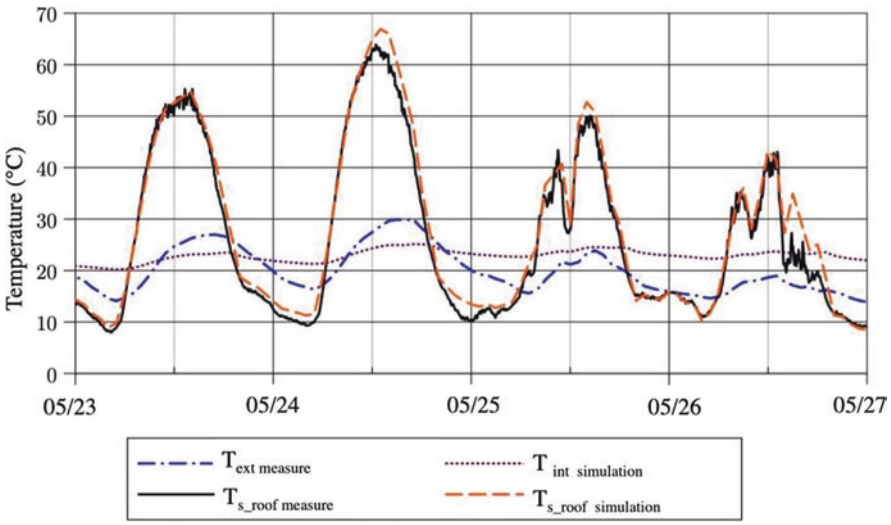

Fig. 13.7 Comparison of measured and simulated roof surface temperature. (Adapted from Malys 2012)

Eight thermocouples were set on this building's roof measuring its temperature over 1 week. The amplitude of the surface temperature daytime variation reached 50 °C during sunny days. For the comparisons, an average of the eight measurements (which were very similar) was used. During the night, the surface temperature was generally lower than the air temperature.

In Fig. 13.7, we compare simulation and measurement. One can verify that there are two short periods during which the model does not well represent the measured values. During the second night, there is a 4 °C difference and at the end of the fourth afternoon there is a 10 °C difference. For the first period, the wind is very weak and the CHTC calculated considering forced regime is certainly underestimated. For the second period, we think that the 1-h time step used for simulation does not permit to catch the impact of changing weather and in particular varying solar fluxes. Apart from these differences, the simulation results are close to the measurements and the daily variation well reproduced.

During the three days of the campaign (May 21st to 24th), the surface temperatures of several surfaces have been manually acquired using a radiometer. Unfortunately, indoor temperatures have not been recorded. For comparison, we use the temperatures measured on a south-facing facade of a building identical to the previous one.

Two kinds of simulations are carried out. For the first one, the building surface temperatures are calculated using the wall model presented above with fixed indoor air temperature (20 °C) as boundary condition of the 1D thermal model for each mesh element. For the second one, we apply the simplified building energy model

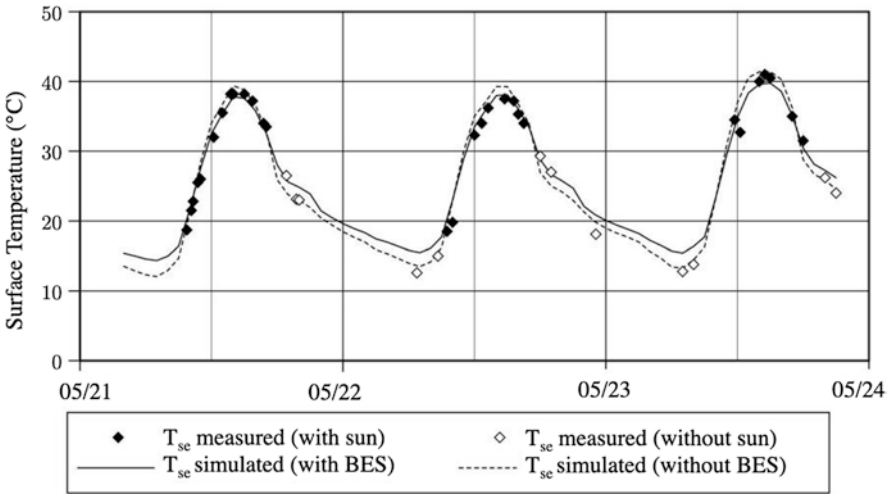

Fig. 13.8 Comparison of measured and simulated facade surface temperature. (Adapted from Malys 2012)

(BEM) that will be presented later (Sect. 13.6.1) and calculate the indoor temperature for each floor (free-running mode). In Fig. 13.8, one can notice that facade's temperatures are lower than the roof's. When applying the BEM, the surface temperature is well assessed when the wall is insolated, but the assessment is worse otherwise. It is the contrary when we do not use the BEM. One explanation could be the simplification that has been done in the BEM when gathering all the internal surface nodes in a unique one for each floor (Bouyer et al. 2011) as it will be shown later in Sect. 13.6.1. However, the model represents well the surfaces' temperature variations.

Finally, the detailed soil model performance has been assessed in an open space (a car park). This case study has been selected to avoid the influence of the surrounding surface on the module evaluation. The simulated temperatures have been compared to the measurements in situ. The mean daily RMSE between the estimated and the observed surface temperature is 0.86, 0.72, 0.58, 0.26, and 0.13 °C, respectively, at the surface, 5, 10, 34, and 50 cm depths. Details can be found in the work of Azam et al. (2018b).

13.4 CFD Coupling

The coupling of the SOLENE model with a CFD model was first performed by Vinet using the N3S CFD code, which has been replaced by FLUENT (Robitu 2005) and later by Code_Saturne (http://code-saturne.org/cms/) (Qu et al. 2012).

The coupling principle was detailed by Bouyer et al. and offers three possibilities (Bouyer et al. 2011):

1. Full dynamic coupling (CFD/thermo-radiative iterations until strict convergence), which was used by Robitu et al. (2006), taking into account the buoyancy effect in CFD: After these first attempts, the high CPU usage was judged very high and could be justified for some specific comfort issues.
2. Quasi-dynamic coupling (only one iteration for both CFD/thermo-radiative simulations): Potentially insufficient to obtain a complete retroactive effect on surface temperatures in the thermo-radiative simulation, this coupling is also insufficient to strictly represent heat and moisture transport in CFD.
3. An intermediate coupling approach proposed by Bouyer et al. (2011) (Fig. 13.9), whereby the resolution of momentum, continuity, and turbulence equations is disabled after the initialization process: Velocity and turbulence fields are preprocessed for each wind direction and velocity. Then, for each time step during the iterative process, only transport equations for energy and moisture are solved. The computational cost is considerably reduced. This intermediate approach is tantamount to assuming that airflow is not disturbed by heat transfer at the wall

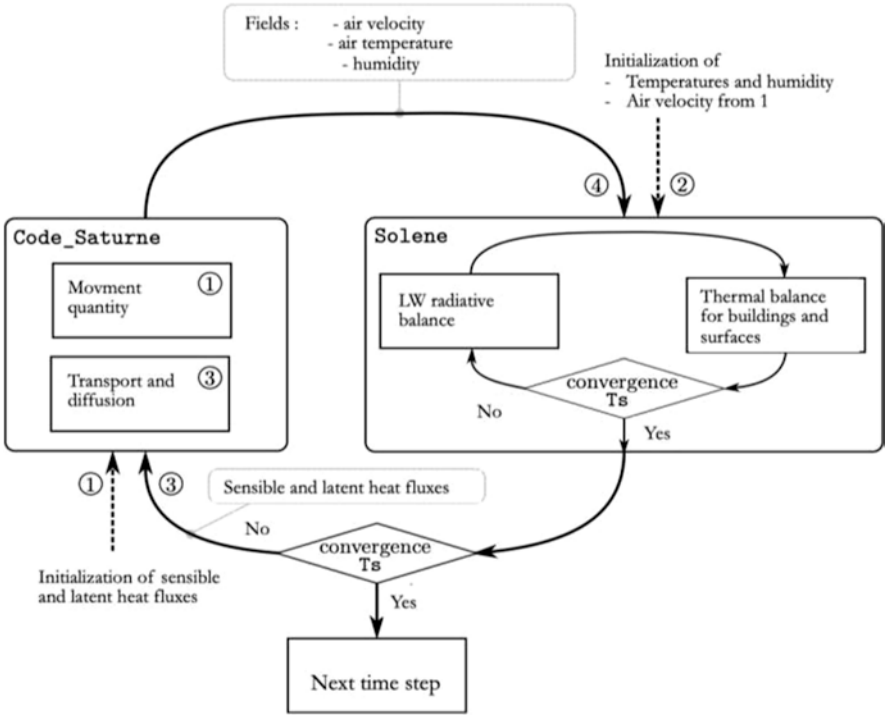

Fig. 13.9 Flowchart of a time step coupling SOLENE and Code_Saturne

surface. Doing that, the impact of insolated walls on airflow will be inaccurate and local recirculation can cause locally high temperatures that would not happen due to buoyancy effect. This will not have a significant effect on buildings' thermal behavior but will affect local comfort assessment.

CFD coupling is also employed to compute the moisture transfer and diffusion of natural surfaces.

In practice, the variables exchanged between the CFD and the thermo-radiative model are as follows:

- From CFD to *the thermal model*:
  - Near-surface air velocity used to calculate the CHTC required for the surface energy balance equation: For this purpose, the linear law derived by Jayamaha et al. has been chosen (Jayamaha et al. 1996) (Eq. 13.5).
  - Near-surface air temperature, which is also required to calculate convective heat flux at the wall surface (in addition to evaluating the sensitive ventilation load).
- From the thermal model to CFD:
  - The convective heat fluxes affecting the energy transport equation and the moisture mass transfer.

Starting from the third coupling method, the impact of coupling with CFD on the assessment of the energy demand of one building in an urban environment has been studied by Malys et al. (2015). In that paper, a sensitivity analysis has been carried out to determine whether the use of local temperature and wind speed was necessary to calculate the convective heat flux. It concludes that for building energy simulation purposes and under winter conditions, thermal coupling with the aerodynamic model in order to represent neighborhood effects can be avoided by using mean values for wind speed and local air temperature. This is less the case during summer since the solar irradiance on surfaces and convective phenomena modify the local temperature in higher proportions.

For winter and energy purposes, a method has been proposed to take into account the impact of the surfaces' temperature on air temperature, and vice versa, in a simple manner. It consists of considering a control volume in which it is assumed that the air temperature is homogeneous. Then, a thermal balance to the air mass contained in this volume is done. The temperature of entering air is considered to be the meteorological temperature, whereas the temperature of exiting air is the mean temperature of the control volume. The airflow entering the volume is calculated by integrating the wind profile (Malys et al. 2015). In this method, the thermo-radiative model is used, without the coupling to the CFD, but a local air temperature can be taken into account.

13.5 Climate Adaptation Techniques

13.5.1 Vegetation

Several green devices have been modeled: trees, lawns, green roofs, and green walls.

Trees are considered as a surface in the radiative model (the tree crown envelop) and as a volume in the CFD model (Fig. 13.10) (Robitu et al. 2006). The impact of trees on the radiative environment is considered taking into account their shading and sun radiation absorption. The tree surface has a solar transmission, reflection, and absorption. It is opaque to long-wave radiation and emits long-wave radiation according to its surface temperature.

In the CFD model, the tree volume contains an aerodynamic resistance. The cells it contains are considered as mixed air/foliage volumes with only one mean temperature for the two entities. This one is calculated as the result of an energy balance equation applied to each tree cell, taking into account radiative fluxes coming from the radiative model (only for cells adjacent to the external surface of the tree), and latent and convective energy exchanges (Bouyer 2009).

Malys introduced green roofs and walls as well as lawns. Unlike trees, these models do not require the addition of a specific entity but are complementary equations added to the wall, roof, and soil models so as to represent the role of foliage in the surface-to-air interface (Fig. 13.11) (Malys et al. 2014). Foliage acts as a partial barrier to radiation. It exchanges with both the surface that supports it (the substrate when present or directly the wall in case of climbing plants) and the surrounding surfaces. It also exchanges convective and latent heat fluxes. For these kinds of surface, the latent heat flux of the substrate is also considered when there is a substrate. As SOLENE-microclimat does not include a hydrological model, this one is

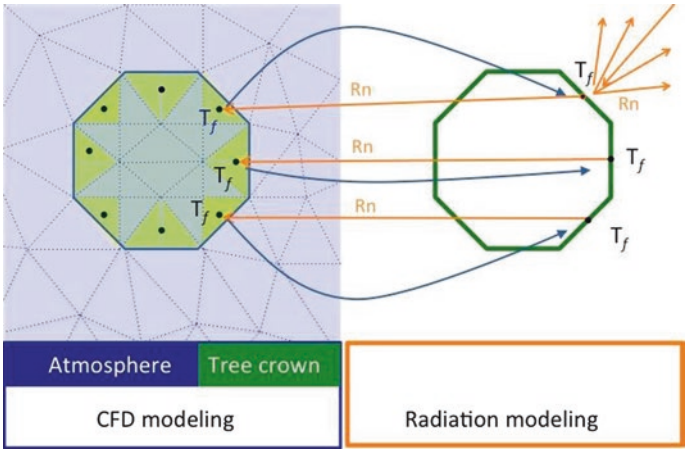

Fig. 13.10 Model used to represent the thermal behavior of trees. (Adapted from Robitu 2005)

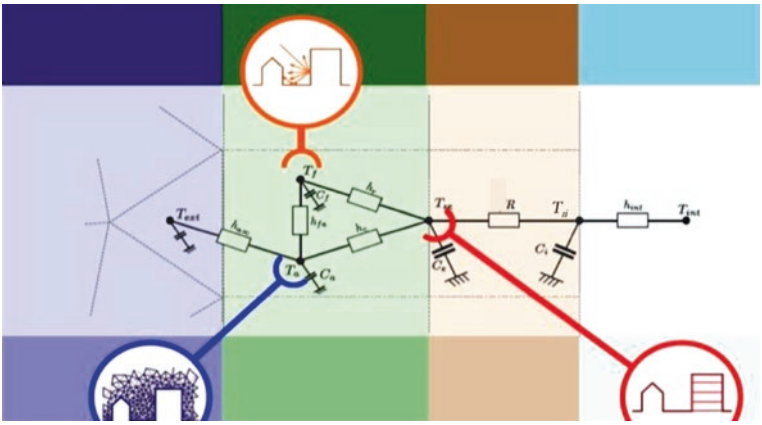

Fig. 13.11 Nodal model used to represent the thermal behavior of green walls and roofs. (Adapted from Malys 2012)

controlled by an evapotranspiration rate (*f*). It is introduced to consider the occurrence of water stress within the substrate (Eqs. 13.6 and 13.7). The distribution of this flux between the foliage and the substrate is realized through the coefficient α_{lat}:

$$LE_f = \alpha_{lat} f ETP \tag{13.6}$$

$$LE_s = (1 - \alpha_{lat}) f ETP \tag{13.7}$$

The method adopted to calculate evapotranspiration (ETP) is based on the Penman-Monteith equation, as advised by the Food and Agriculture Organization (FAO).

Latent fluxes from vegetation and its substrate are used to calculate the mass rate of moisture released into the air and taken into account in the CFD model.

Malys (2012) drew an initial comparison between the results obtained for green walls and the experimental data recorded by HEPIA, which showed a good agreement.

A comparison has also been carried out for soils covered by lawn as a part of VegDUD project (Musy et al. 2015). The measurement was conducted in the Pin Sec district (in Nantes, France) using Taupe recorders with three sensors at the depths of 0, −5, and −35 cm and at two different locations. The comparison between simulation and measures showed that the simulation reproduces well the surface temperature on sunny days, but also that the model seems to overestimate the nocturnal cooling.

The models used for trees and green roofs have not yet been validated, although temperatures obtained for tree volumes are close to air temperature, as found in the literature.

13.5.2 Water Ponds

To evaluate the impact of water ponds on outdoor thermal comfort, a thermal model developed by Robitu et al. (2004) considers the radiation absorbed, transmitted, and reflected at the water surface. The fraction of absorbed radiation raises the water temperature and the transmitted fraction reaches the bottom of the pond.

The factors affecting solar radiation attenuation in water ponds (spectral distribution of water properties, angle of incidence, water-layer thickness, and reflectivity of pond bottom) are taken into account using the model proposed by Cengel and Özişik (1984). The absorption coefficient is highly dependent on the wavelength; in this submodel, the solar spectrum was divided into 20 bands so that extinction coefficients corresponding to these bands match those from Cengel and Özişik (1984).

Once the solar radiation for each band is known, the part reaching the bottom and the part at various pond depths are summed to obtain the total flux absorbed at each depth in water. Conduction and heat storage in water are solved by using finite difference method (Fig. 13.12).

The water pond model has not been assessed yet, but the impact of such a device has been simulated in an existing place by Robitu et al. (2004). It has been shown that the effect of water ponds is mainly local. The water surface has a local impact on air humidity and temperature. But for comfort assessment, as the radiation budget is not significantly changed for an individual exposed to sun, this impact is very low.

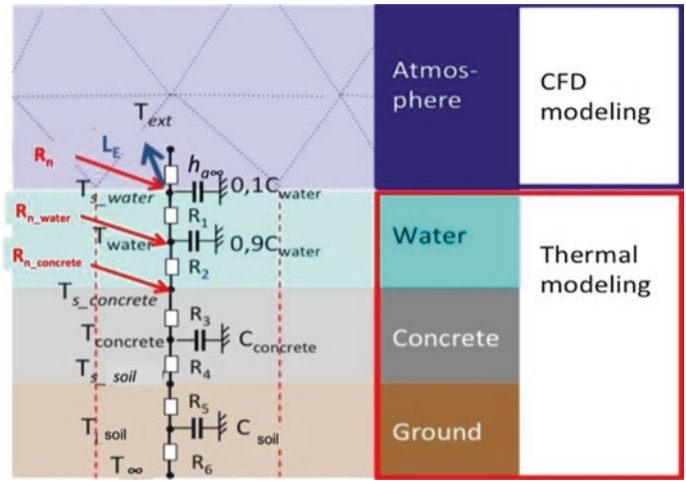

Fig. 13.12 Water pond model illustrated with one intermediate water node

13.5.3 Pavement Watering

A module to simulate the behavior of watered surfaces has been developed. Watering events are modeled through a runoff convective heat flux noted $Q_{\text{wat - pav}}$ and a latent heat flux noted LE (Fig. 13.13). Equation (13.4) is then modified to include these two heat fluxes (Eq. 13.8):

$$Q_{\text{cond}} = R_{\text{n}} + H - \text{LE} - Q_{\text{wat-pav}} \tag{13.8}$$

$$Q_{\text{wat-pav}} = \frac{\rho_{\text{w}} C_{\text{p,w}} \cdot h_{\text{w}}}{\Delta t}\left(T_{\text{s}} - T_{\text{water}}\right) \tag{13.9}$$

The runoff convective heat flux represents the sensible heat exchanged between the soil surface and the water layer (Eq. 13.9). The latent heat flux can then be calculated from the available water height at the surface and the potential latent heat flux (noted LE_{th}). If the potential evaporation water height (noted $h_{\text{evap, th}}$, given by Eq. 13.12) is higher than the available water height (noted h_{w}), all the water present at the surface evaporates. Then Eq. (13.10) is used. However, if the potential evaporation water height is smaller than the available water height, only a part of the water layer evaporates. Then Eq. (13.11) is used:

$$\text{LE} = \text{LE}_{\text{th}} \frac{h_{\text{w}}}{h_{\text{evap,th}}} \tag{13.10}$$

$$\text{LE} = \text{LE}_{\text{th}} \tag{13.11}$$

$$h_{\text{evap,th}} = \frac{\text{LE}_{\text{th}} \Delta t}{L \cdot \rho_{\text{w}}} \tag{13.12}$$

If the simulation time step is small (i.e., 15 min), both heat fluxes are added one at a time as presented in Fig. 13.13. However, for larger time steps (i.e., 1 h), both latent and runoff convective heat fluxes are added at the same time. At each time

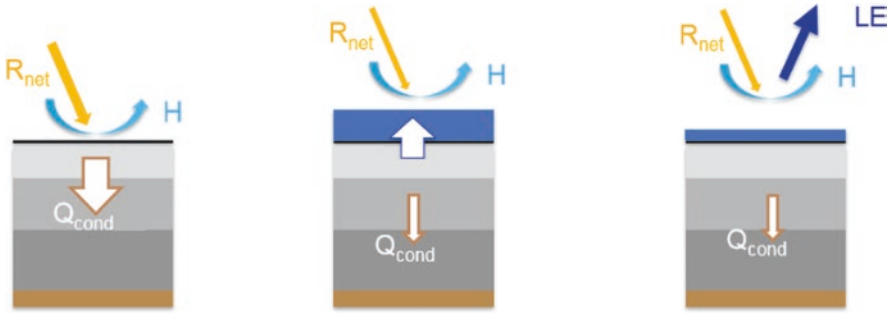

Fig. 13.13 Pavement watering heat flux decomposition

step, the water layer available at the soil surface is monitored for each piece of the mesh.

This watering model has been evaluated using the data from a measurement campaign performed on an asphalt car park during warm days. The measurement campaign reveals that the surface cooling is mainly due to evaporation (80%). However, under warm conditions, the heat flux exchanged between the runoff water and the surface should also be modeled. The mean daily RMSE between estimated and observed surface temperature is 1.04, 0.86, 0.66, 0.35, and 0.21 °C, respectively, at the surface, 5, 10, 34, and 50 cm depths. Details on the model and its assessment can be found in the work of Azam et al. (2018a).

This watering model has also been applied in an urban context, to model pavement watering of a street in the La Part-Dieu district in the city center of Lyon. The model performances are assessed on two hot, clear, and sunny days. Simulated and measured in situ surface temperatures as well as radiation measurements are compared. A RMSE of 2.99 °C is observed, without calibration of the thermal properties of the urban scene. With this model, the effect of pavement watering on soil temperature can be evaluated. In this specific case, an evening watering scenario (17–22 h GMT) decreases the surface temperature by 4.09 °C. Details on this practical example can be found in the work of Azam et al. (2019).

13.6 Assessment Modules

SOLENE-microclimat allows assessing the impact of urban forms, materials, or climate adaptation solutions on both indoor and outdoor conditions. The study of indoor impacts (building's energy consumption or indoor thermal comfort) uses a building energy model while the study of outdoor thermal comfort can be carried out thanks to different outdoor comfort models.

13.6.1 Building Energy Model (BEM)

13.6.1.1 Model Description

Two options are available for the BEM coupling. The first one was presented in detail by Bouyer et al. (2011); it consists of a submodel for SOLENE and it is based on a multizonal building nodal network, whose nodes correspond to the building floors (Fig. 13.14). All the external facets are assigned to a floor and linked at the internal surface so that conductive fluxes (and transmission through the windows) contribute to the floor energy balance equation. Indoor temperatures or heating or cooling power necessary to maintain indoor temperature at a set point can then be calculated.

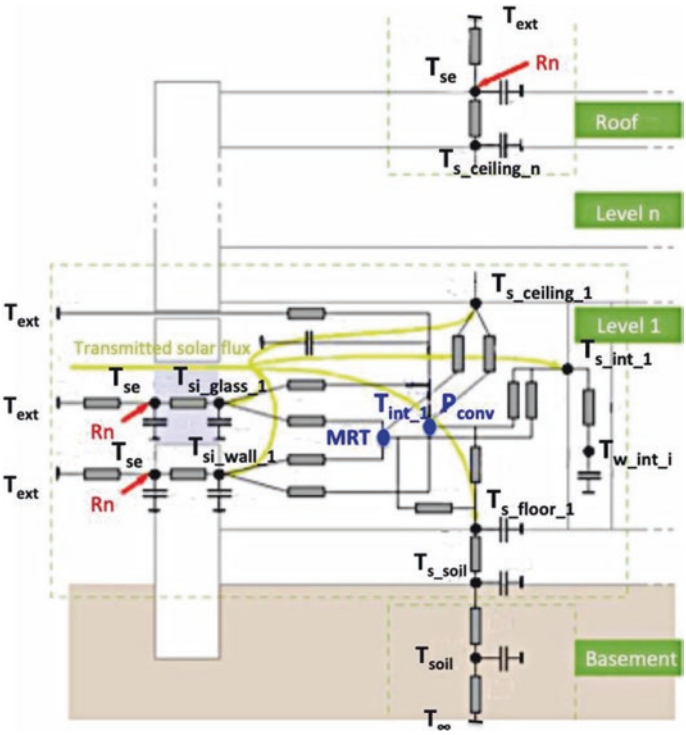

Fig. 13.14 Simplified BEM in SOLENE-microclimat (scheme adapted from Bouyer 2009) resistances and capacities have not been noted in the interest of clarity. It must also be noted that the external nodes are duplicated as many times as the number of external nodes per external surfaces

The second model, called DANA (DetAiled buildiNg simulAtion), has been presented by Rodler et al. (2018). Here, the building's indoor surfaces are differentiated so that the internal surface temperature is calculated for different orientations (Fig. 13.15). In this model, the urban geometry is composed of facets, triangular mesh elements, and cells. To illustrate these terms, some of the facets of the geometry are surrounded in brown in Fig. 13.15. DANA model can represent the dynamic thermal behavior of a single building of any shape using a multizone approach, where each level is a zone. Internal gains and the air leakage through the external envelope are considered. Heating and cooling needs are calculated as well as the air and radiant temperatures for each floor. The external surface temperatures are calculated, with SOLENE-microclimat, for each mesh element of the urban geometry, as we consider the discretized boundary conditions. The thermal conduction exchanges in the walls are still considered unidimensional but the spatial discretization within the walls is refined.

This model can be used as a stand-alone BEM model or can be coupled to SOLENE-microclimat by a weak coupling. The latter consists of, for a time step, launching first the thermo-radiative model whose facade temperatures are used as

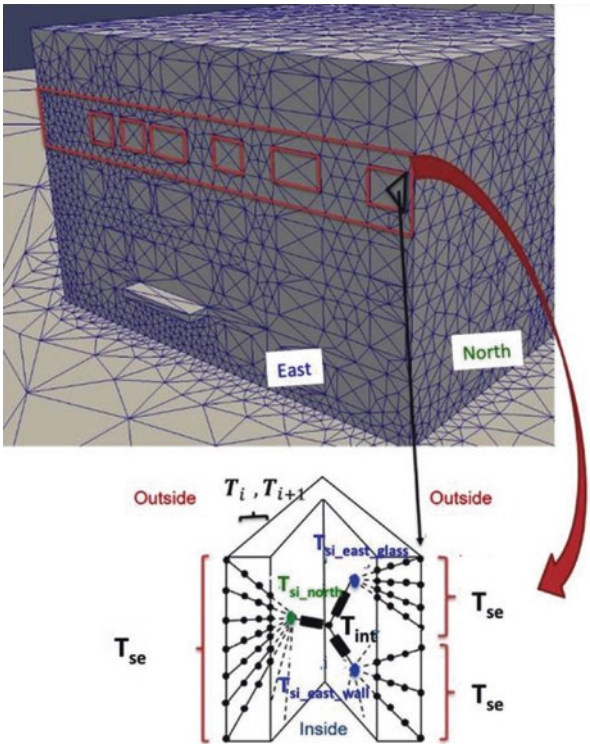

Fig. 13.15 Detailed building energy module DANA: Urban geometry elements: facets, triangular mesh elements, and cells. (Adapted from Rodler et al. 2018 with permission). On each external facet, a surface balance equation is written implying the net radiation, convective, and conductive fluxes, while the internal gains and HVAC loads are applied to the zone (floor) internal air node

initialization to the building energy model DANA. Second, once DANA has finished the resolution of the energy balance, the new calculated buildings outside surface temperatures are used as input to the thermo-radiative function. Then, the resolution can move to the next time step. CFD can be added to the coupling process if the user needs it. If it is the case, the modeler should launch the CFD with the thermo-radiative calculation. In any case, DANA will use all the other fluxes coming from the CFD and the thermo-radiative function, such as long-wave, short-wave, and sensible heat fluxes.

13.6.1.2 Model Assessment

The first approach has not been validated but the walls' and roofs' external surface temperatures were compared to measurements made during the FluxSap campaign as explained above, which led to revising of the model and proposing of a more detailed version.

The results obtained with the second one have been compared to data acquired in the long-term monitoring of a building and the ones that surround it. The comparison was focused on the outside surface temperatures of several buildings within the district, inside air temperatures, and surface temperatures of four flats of the last

floor of the central building (which was more intensely equipped with sensors), and its energy demand during winter. They were compared to measures and showed a good agreement (Rodler et al. 2018).

13.6.2 Thermal Comfort Modeling

Several thermal comfort models have been implemented. First, they require calculating the mean radiant temperature (MRT) in the scene. It was performed by Vinet (2000) through defining the so-called bonhomme confort (Fig. 13.16). It is a human representative geometry on which MRT is calculated. For that purpose, all long-wave exchanges between the cylinder representing the human body and all the surfaces, including the sky, are calculated as well as short-wave flux directly from the sun or from the surfaces after multiple reflections with the radiative model presented above. This leads to the calculation of MRT described in the next equation:

$$\mathrm{MRT}^4 = T_1^4 F_{p-1} + T_2^4 F_{p-2} + \cdots + T_n^4 F_{p-n} \tag{13.13}$$

where MRT is the mean radiant temperature of the body, T_n the temperature of the surfaces seen by the body, and F_{p-n} the view angle between the body and the surface seen by the body. This value in turn leads to evaluating various comfort indices: predictive mean vote, PMV* (Robitu 2005); physiological equivalent temperature, PET (Athamena 2012); and universal thermal climate index, UTCI (Weihs et al. 2012).

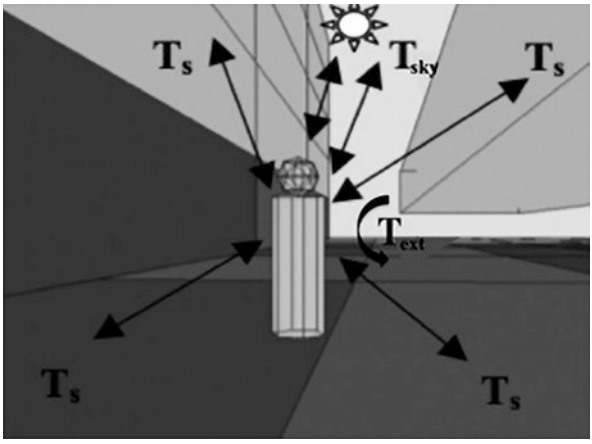

Fig. 13.16 "Bonhomme confort" and the exchanges occurring with its environment

13.7 Applications

Hereafter, the application of the model to the assessment of adaptation strategies' efficiency with regard to outdoor or indoor comfort is described.

13.7.1 Comparison of Different Urban Cooling Strategies Regarding Pedestrian Comfort

The objectives of the EVA project were to compare three different urban cooling strategies: the use of water aspersion systems, vegetation, and high-albedo materials. We present here the results focusing on outdoor thermal comfort.

The assessment of the different cooling strategies was carried out through a set of simulations designed to explore different configurations:

- Cooling strategies were first applied individually to each district so as to compare their impact.
- A composition of the three strategies is then considered trying to optimize their effect (optimized scenario).
- The contribution of each solution to the optimized scenario is finally investigated by deducing it from the optimized configuration (subtractive scenario). This also allows evaluating the cumulative effect of solutions.

The study was applied to three districts in Lyon:

- The Frankfort Square, a multimodal square in front of the La Part-Dieu train station
- The Moncey buildings' block (part of a residential district built in the 1960s)
- The Buire street (part of a recent residential district)

The three districts and the optimized scenarios are presented in Fig. 13.17. The spaces highlighted in red will be studied more in detail regarding pedestrians' comfort. Water aspersion systems are the blue surfaces, vegetation (trees, green walls, or

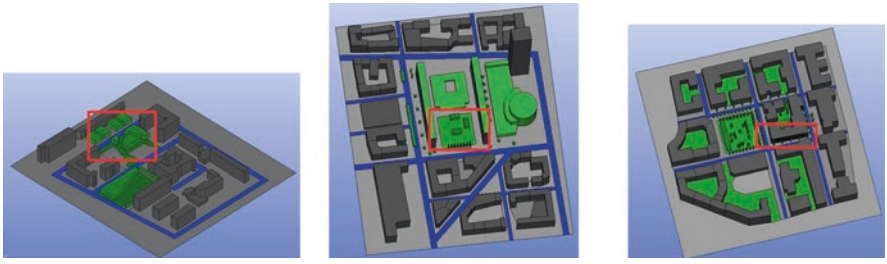

Fig. 13.17 Representation of the optimized scenario applied in the Frankfort district (left), the Moncey district (center), and the Buire district (right)

roofs), and the green ones. The materials are classified based on three albedo levels: low albedo: 0.15; medium albedo: 0.4; and high albedo: 0.8. To produce the high-albedo scenario, for each surface family (roads, buildings, roofs), the albedo value is modified from its actual estimated level to the immediately higher albedo value category.

The simulations are performed using the meteorological data from the heat wave that occurred in July 2003 (26th).

13.7.1.1 Influence on Air Temperature

The results show a reduction of the air temperature at pedestrian height (1.5 m) for each cooling strategy applied individually (Fig. 13.18). High-albedo materials slightly reduce the air temperature but the effect is more widely spread. The reduction induced by the water aspersion systems is higher but concentrated near the space where they are applied. Vegetation also significantly reduces the air temperature in the space where it is applied. It can also induce a slight air temperature increase because of the reduction of the wind speed, which modifies convective exchanges and thus surface temperature. Similar results were observed for all the districts.

13.7.1.2 Influence on Thermal Comfort

The influence of the cooling strategies on thermal comfort is investigated by analyzing the optimized scenario and the subtractive ones (Fig. 13.19). In Fig. 13.19, the dark line with dark points presents the evolution over the day of the average UTCI values for each studied area.

The bars give the contribution of each cooling solution. For each cooling solution, it has been calculated by comparing the UTCI from the optimized scenario with the one from the scenario in which this solution has been deleted. The dark crosses represent the sum of the contributions.

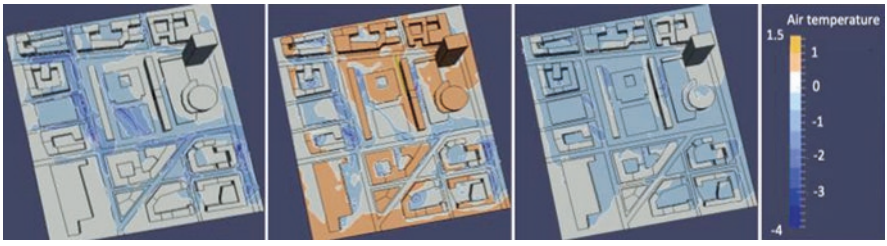

Fig. 13.18 Reduction of air temperature for each cooling strategy applied in the Moncey district at midday. Water aspersion (left), vegetation (center), high-albedo materials (right)

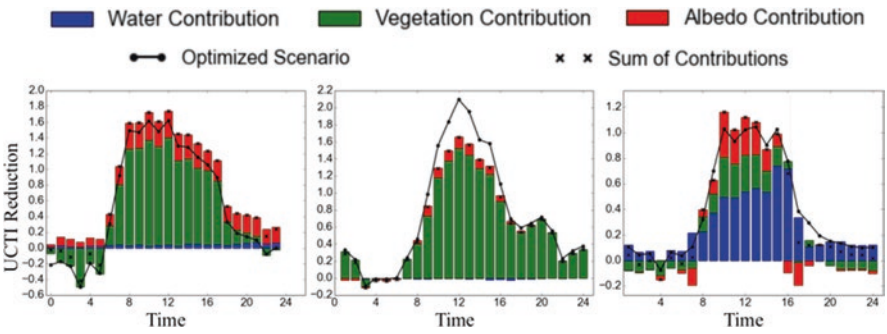

Fig. 13.19 Reduction of UTCI mean values for the studied area in each district: Frankfort (left), Moncey (center), and Buire (right)

The crosses do not match with the points. This means that the total UTCI reduction cannot be considered as the sum of every single effect: the effects are not completely additive. Secondly, the contribution of each cooling strategy as well as its efficiency is different depending on the district. The vegetation has a higher contribution to the optimized solution, especially in the Frankfort place and the Moncey district. As previously presented, vegetation (and in particular trees) can induce a negative influence. Even if they have a positive influence on average where they are applied, in the three cases, trees induce negative effects at nighttime (not visible in Moncey district where few trees were implemented) because they reduce the cooling by infrared radiation exchanges with the sky. Thirdly, the water contribution is low in two of the three cases because it has been implemented on a few surfaces and at such a distance from the studied place that one can only observe the indirect impacts. Lastly, albedo value increase can have a positive or a negative influence, depending on the hour of the day and even more on the urban configuration.

The results of these investigations show that the efficiency of the cooling strategies is very different depending on the district configuration, on the way they are applied, and on the interactions between them. Effects are not additive; they also vary over the day, and can be negative at some times and places. One must also consider that effects on air temperature must be distinguished from those on thermal comfort that encompass several phenomena (air temperature, humidity, radiation, and wind speed). This confirms the difficulty to produce general rules and the need for tools to specifically study each new configuration.

13.7.2 Comparison of the Effect of Green Devices on Indoor Comfort

SOLENE-microclimat, with green roofs, green walls, and lawns, has been applied to the analysis of summer conditions for Pin Sec district of Nantes city (France) (Malys 2012). The effects of green roofs, green walls, and lawns on indoor comfort

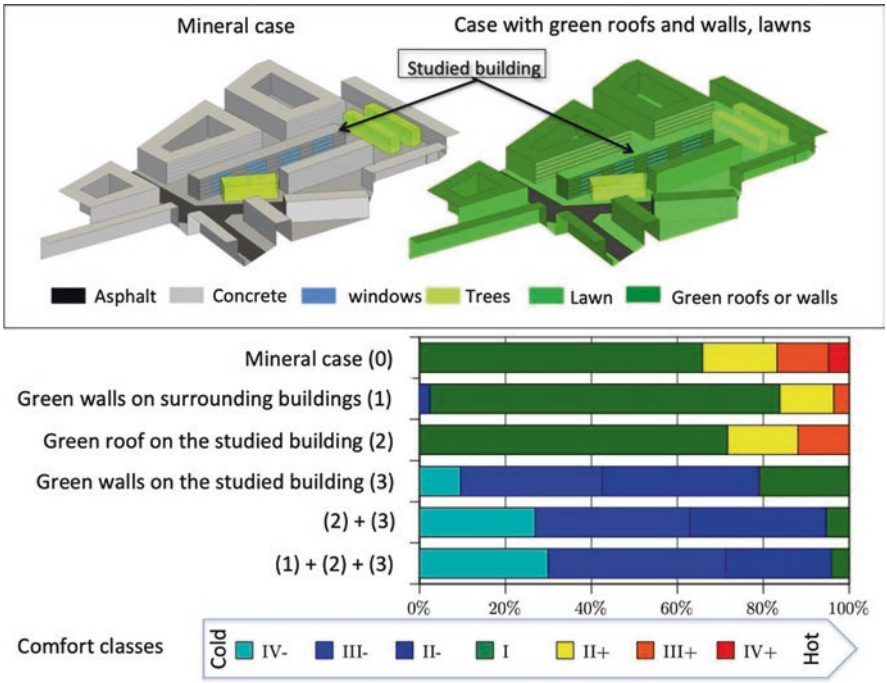

Fig. 13.20 Top: the two extreme cases, case (0) and case (1)+(2)+(3); bottom: the results in terms of percentage of time in each adaptive comfort class over a day

in two kinds of buildings (i.e., insulated or not) taken individually have been compared. First, it has been verified, as often underlined in literature, that green solutions mainly affect non-insulated buildings (Malys et al. 2016). Secondly, it has been demonstrated that the model allowed separating direct and indirect effects of green roofs and walls by simulating successively the implementation of vegetation on the studied building (cases 2 and 3) and on the surrounding (case 1) (Fig. 13.20).

The results are hereafter analyzed for the second floor and in terms of adaptive comfort (Malys et al. 2016). They show that green roofs mainly have a direct effect on the buildings where they are installed, with this effect essentially being verified on the top floor due to the direct shading of the foliage. Comparing reference case to case 2, in Fig. 13.19, one can notice that for the second floor, the comfort is slightly improved. Not represented here, the simulations showed that the indirect effect was very small as the result of a limited effect on air temperature (it has also been verified by de Munck 2013) and due to the fact that buildings are of equal height, so that their roofs have no long-wave radiative effect on the other buildings.

Comparison of reference case, case 1, and case 3 shows that green walls have direct and indirect effects. The direct one is greater due to the effect of shading foliage, while indirect effect is due to the lower radiant flux exchanged with the surrounding buildings.

When the building already benefits from the direct effect of green walls, the addition of green walls on the surrounding buildings has a low effect on indoor comfort (comparison of case 1+2+3 and case 2+3).

13.8 Conclusion

Urban microclimate simulation and building energy simulation at the district scale, including impacts of surrounding areas, are highly anticipated by professionals and should experience the kind of rapid expansion that building energy simulation underwent over the past decades. It is thus necessary to propose models that are both robust (in terms of the cases it can treat) and validated.

The more the expected expertise will concern local comfort adaptation strategies, the more the models will have to accurately represent local variables (surface temperature, air temperature and humidity, wind velocity). We showed that this requires having an accurate representation of phenomena such as mixed convection, long-wave and short-wave radiative exchanges, conduction in materials, and evapotranspiration.

For that purpose, SOLENE-microclimat has become increasingly comprehensive and now contains a detailed description of urban areas. A systematic step of validation has also been instanced so as to ensure the reliability of models.

However, for applications at a larger scale (for instance, the comparison of different master plans) a compromise must be found that considers modeling accuracy, computing capabilities, and data availability. It is the reason why we consider two development strategies:

- The first one consists of continuing to develop accurate submodels that we validate and that will serve as reference to qualify the simpler ones we keep for rougher applications.
- The second one consists of working on models' reduction as already done for the soil model (Azam et al. 2018c) so as to reduce simulation duration while keeping a good accuracy of phenomena.

For the moment, as most of the developers of urban climate models, one difficulty we have to overcome is the lack of reliable input data, at the city scale as well as at the building scale. With the increasing concern about urban climate, the effort put on the coordination between simulation tools and urban databases will provide the documentation necessary to represent urban microclimate characteristics in greater detail. This breakthrough will certainly be very valuable in terms of understanding and knowledge of underlying phenomena, in addition to highlighting the various impacts of urban parameters (the type of buildings, the land use, and the behavior) on climate at different scales.

Nomenclature

$C_a/C_f/C_s/C_e/C_i$	Thermal capacity of air/foliage/soil/external layer/internal layer (J K^{-1})
$C_{water}/C_{concrete}/C_{soil}$	Thermal capacity of water/concrete/soil layer (J K^{-1})
e	Wall thickness (m)
ETP	Reference evapotranspiration (kg m^{-3} s^{-1})
F_{ij}	Form factor of surface j from surface i (−)
f	Evapotranspiration rate (−)
H	Convective heat flux density (W m^{-2})
$h_{a\infty}/h_{int}$	External/internal convective heat transfer coefficient (W m^{-2} K^{-1})
$h_{fa}/h_f/h_c$	Heat transfer coefficient within a green roof or wall, between foliage and air/foliage and wall/air and wall
LE	Latent heat flux density (W m^{-2})
MRT	Mean radiant temperature (K)
P_{conv}	Heating load (W)
$R_{direct\_SW}/R_{diffuse\_SW}/R_{IR\_SW}$	Direct/diffuse/from interreflection, incoming SW radiative heat flux
R_n	Radiative net heat flux density (W m^{-2})
$R_{n\_water}/R_{n\_concrete}$	Radiative heat flux absorbed by the water layer/concrete layer
T_a	Temperature of air within the tree canopy (K)
T_{ext}/T_{int}	External/internal air temperature (K)
T_f	Foliage temperature (K)
$T_{s\_water}/T_{s\_concrete}/T_{s\_soil}/$ $T_{s\_roof}/T_{s\_ceiling}/T_{s\_floor}/T_{s\_wall}$	Temperature of the upper surface of water/concrete/soil/roof/ceiling/floor/wall (K)
$T_s/T_2/T_3/T_\infty$	Temperature of ground from external surface to reference point (K)
T_{se}/T_{si}	Temperature of wall external/internal surface (K)
$T_{water}/T_{concrete}/T_{soil}$	Water/concrete/soil layer temperature (K)
V_a	Air velocity (m s^{-1})
α_i	SW absorption coefficient of the surface (−)
ε_i	Emissivity of the surface (−)
σ	Stefan-Boltzmann constant (W m^{-2} K^{-4})
$Q_{wat\text{-}pav}$	Runoff sensible heat flux density (W m^{-2})
ρ_w	Water density (kg m^{-3})
$C_{p,\,w}$	Water specific heat (J kg^{-1} K^{-1})
h_w	Water height over the surface (m)
Δt	Simulation time step (h)
L	Latent heat of the vaporization of water (J kg^{-1})

Acknowledgments The development of SOLENE-microclimat has been conducted within the framework of several research projects and Ph.D. theses. We would like to thank ADEME and Région des Pays de la Loire (L. Malys Ph.D., EVA project—contract XXX), Agence Nationale de la Recherche (VegDUD project—contract ANR-09-VILL-0007), Université de Nantes (M. Robitu Ph.D.), CNRS (J. Bouyer Ph.D.), European Community (Built2Spec Project—GA No. 637221–H2020-EeB-2014-2015), and Ecole Nationale Supérieure d'Architecture de Nantes that supported and hosted most of the developments until 2016.

References

Athamena, K. (2012). *Modélisation et simulation des microclimats urbains: Étude de l'impact de la morphologie urbaine sur le confort dans les espaces extérieurs. Cas des éco-quartiers*, Thèse de Doctorat, Ecole Centrale de Nantes & CSTB. Retrieved from https://tel.archives-ouvertes.fr/tel-00811583

Azam, M.-H., Bernard, J., Morille, B., Musy, M., & Andrieu, H. (2018a). A pavement-watering thermal model for SOLENE-microclimat: Development and evaluation. *Urban Climate, 25*, 22–36. https://doi.org/10.1016/j.uclim.2018.04.005.

Azam, M.-H., Morille, B., Bernard, J., Musy, M., & Rodriguez, F. (2018b). A new urban soil model for SOLENE-microclimat: Review, sensitivity analysis and validation on a car park. *Urban Climate, 24*, 728–746. https://doi.org/10.1016/j.uclim.2017.08.010.

Azam, M.-H., Guernouti, S., Musy, M., Berger, J., Poullain, P., & Rodler, A. (2018c). A mixed POD–PGD approach to parametric thermal impervious soil modeling: Application to canyon streets. *Sustainable Cities and Society 42* (1 octobre 2018): 444–61. https://doi.org/10.1016/j.scs.2018.08.010

Azam, M.-H., Rodler, A., Musy, M., Morille, B., & Guernouti, S. (2019). A pavement-watering thermal model validation for SOLENE-microclimate: application to the Buire street. 5th International Conference on Countermeasures to Urban Heat Islands (IC2UHI), Hyderabad, India.

Bouyer, J. (2009). *Modélisation et simulation des microclimats urbains—Étude de l'impact de l'aménagement urbain sur les consommations énergétiques des bâtiments*, PhD thesis. Ecole Polytechnique de l'Université de Nantes.

Bouyer, J., Inard, C., & Musy, M. (2011). Microclimatic coupling as a solution to improve building energy simulation in an urban context. *Energy and Buildings, 43*(7), 1549–1559. https://doi.org/10.1016/j.enbuild.2011.02.010.

Cengel, Y. A., & Özişik, M. N. (1984). Solar radiation absorption in solar ponds. *Solar Energy, 33*(6), 581–591. https://doi.org/10.1016/0038-092X(84)90014-8.

de Munck, C. (2013). *Modélisation de la végétation urbaine et stratégies d'adaptation pour l'amélioration du confort climatique et de la demande énergétique en ville*, PhD thesis. Université de Toulouse, Toulouse.

Hénon, A., Mestayer, P., Lagouarde, J.-P., & Voogt, J. (2012a). An urban neighborhood temperature and energy study from the CAPITOUL experiment with the SOLENE model—Part 1: Analysis of flux contributions. *Theoretical and Applied Climatology, 110*, 177–196. https://doi.org/10.1007/s00704-012-0615-0.

Hénon, A., Mestayer, P., Lagouarde, J.-P., & Voogt, J. (2012b). An urban neighborhood temperature and energy study from the CAPITOUL experiment with the SOLENE model—Part 2: Influence of building surface heterogeneities. *Theoretical and Applied Climatology, 110*, 197–208. https://doi.org/10.1007/s00704-012-0616-z.

Jayamaha, S. E. G., Wijeysundera, N. E., & Chou, S. K. (1996). Measurement of the heat transfer coefficient for walls. *Building and Environment, 31*(5), 399–407. https://doi.org/10.1016/0360-1323(96)00014-5.

Malys, L. (2012). *Évaluation des impacts directs et indirects des façades et des toitures végétales sur le comportement thermique des bâtiments*, PhD thesis. Ecole Centrale de Nantes, Nantes, France.

Malys, L., Musy, M., & Inard, C. (2014). A hydrothermal model to assess the impact of green walls on urban microclimate and building energy consumption. *Building and Environment, 73*(0), 187–197. https://doi.org/10.1016/j.buildenv.2013.12.012.

Malys, L., Musy, M., & Inard, C. (2015). Microclimate and building energy consumption: Study of different coupling methods. *Advances in Building Energy Research*. https://doi.org/10.1080/17512549.2015.1043643.

Malys, L., Musy, M., & Inard, C. (2016). Direct and indirect impacts of vegetation on building comfort: A comparative study of lawns, green walls and green roofs. *Energies, 9*(1), 32. https://doi.org/10.3390/en9010032.

Mestayer, P. G., Rosant, J.-M., Rodriguez, F., & Rouaud, J.-M. (2011). La campagne expérimentale FluxSAP 2010: Mesures de climatologie en zone urbaine hétérogène. *Météorologie (Paris), 1925*(73), 34–44.

Miguet, F., & Groleau, D. (2002). A daylight simulation tool for urban and architectural spaces: Application to transmitted direct and diffuse light through glazing. *Building and Environment, 37*(8–9), 833–843. https://doi.org/10.1016/S0360-1323(02)00049-5.

Musy, M., Malys, L., Morille, B., & Inard, C. (2015). The use of SOLENE-microclimat model to assess adaptation strategies at the district scale. *Urban Climate, 14*(Part 2), 213–223. https://doi.org/10.1016/j.uclim.2015.07.004.

Perez, R., Seals, R., Ineichen, P., Stewart, R., & Menicucci, D. (1987). A new simplified version of the Perez diffuse irradiance model for tilted surfaces. *Solar Energy, 39*(3), 221–231. https://doi.org/10.1016/S0038-092X(87)80031-2.

Qu, Y., Milliez, M., Musson-Genon, L., & Carissimo, B. (2012). Numerical study of the thermal effects of buildings on low-speed airflow taking into account 3D atmospheric radiation in urban canopy. *Journal of Wind Engineering and Industrial Aerodynamics, 104–106*, 474–483. https://doi.org/10.1016/j.jweia.2012.03.008.

Robitu, M. (2005). *Etude de l'interaction entre le bâtiment et son environnement urbain: Influence sur les conditions de confort en espaces extérieurs*, PhD thesis. Ecole Polytechnique de l'Université de Nantes.

Robitu, M., Inard, C., Groleau, D., & Musy, M. (2004). Energy balance study of water ponds and its influence on building energy consumption. *Building Services Engineering Research and Technology, 25*(3), 171–182.

Robitu, M., Musy, M., Inard, C., & Groleau, D. (2006). Modeling the influence of vegetation and water pond on urban microclimate. *Solar Energy, 80*(4), 435–447. https://doi.org/10.1016/j.solener.2005.06.015.

Rodler, A., Guernouti, S., Musy, M., & Bouyer, J. (2018). Thermal behaviour of a building in its environment: Modelling, experimentation, and comparison. *Energy and Buildings, 168*, 19–34. https://doi.org/10.1016/j.enbuild.2018.03.008.

Vinet, J., Antoine, M. J., Raymond, F., & Inard, C. (1999). Modelling the impact of urban vegetation to analyse urban microclimate and outdoor thermal comfort. In *ICUC 1999*.

Vinet, J. (2000). Contribution à la modélisation thermo-aéraulique du microclimat urbain. *Caractérisation de l'impact de l'eau et de la végétation sur les conditions de confort en espaces extérieurs*, PhD thesis. Université de Nantes Ecole Polytchnique de l'Univeristé de Nantes, Nantes, France.

Weihs, P., Staiger, H., Tinz, B., Batchvarova, E., Rieder, H., Vuilleumier, L., et al. (2012). The uncertainty of UTCI due to uncertainties in the determination of radiation fluxes derived from measured and observed meteorological data. *International Journal of Biometeorology, 56*(3), 537–555. https://doi.org/10.1007/s00484-011-0416-7.